

Multi-scale computational homogenization of structured thin sheets

To cite this article: M G D Geers *et al* 2007 *Modelling Simul. Mater. Sci. Eng.* **15** S393

View the [article online](#) for updates and enhancements.

You may also like

- [Dynamic modeling and validation of a novel 3-DOF flexible thin sheet nano-manipulator with piezoelectric material bonded](#)
Ning Chen and Peng Yan
- [Welding of thin sheet of Al5456 aluminum alloy by using GTA and GMA welding process](#)
I Ebrahimzadeh, B Sadeghi and H Maddahi
- [Study on vertical printing of thermally driven PLA actuators: residual stress modulation in FDM-based 4D printing](#)
Liulan Lin, Shaolong Qiu and Jiajie Yan

Multi-scale computational homogenization of structured thin sheets

M G D Geers¹, E W C Coenen¹ and V G Kouznetsova^{1,2}

¹ Faculty of Mechanical Engineering, Eindhoven University of Technology, PO Box 513, 5600 MB Eindhoven, The Netherlands

² Netherlands Institute for Metals Research, Mekelweg 2, 2628 CD Delft, The Netherlands

E-mail: m.g.d.geers@tue.nl

Received 29 November 2006, in final form 5 March 2007

Published 1 May 2007

Online at stacks.iop.org/MSMSE/15/S393

Abstract

Structured and layered thin sheets are used in a variety of innovative applications, e.g. flexible displays, rollable solar cells or flexible electronics. Stacks of different materials, with often highly complex interconnects between layers, are thereby used, which are typically loaded in bending combined with intrinsic thermo-mechanical mismatches. As a result, different failure mechanisms at the level of the layered substructure occur, which constitutes a serious reliability concern.

This paper deals with the two-scale homogenization of structured thin sheets, whereby a higher-order through-thickness representative volume element (RVE) is used. The methodology relies on the computational homogenization of the mechanics of microstructures, for which first-order and second-order solution strategies have been developed in the past decade. The upscaling of the deformation of structured thin sheets towards a shell-type continuum is second-order in nature. The higher-order kinematics is defined on the basis of a microstructural RVE, which represents the full thickness of the macroscopic structure and a periodic in-plane cell (e.g. a single pixel in a flexible display). The elaboration of the boundary conditions and the solution of the micro-scale boundary value problem are discussed. The obtained micro-scale stress state is homogenized towards a 3D macroscopic shell structure, for which detailed aspects will be emphasized. The coupled numerical solution strategy is briefly outlined. Finally, an example is given and the application to a number of practical problems is highlighted, where the solution provides direct information on each scale. The incorporation of failure events at the substructure level is thereby naturally at hand.

(Some figures in this article are in colour only in the electronic version)

1. Introduction

In the past few decades, considerable progress had been made in bridging the mechanical engineering aspects of materials to the field of materials science. This is mainly due to a fruitful combination of micromechanics and multi-scale approaches, with a steadily increasing multi-disciplinary character. Several improved micromechanical theories and associated numerical models have been proposed and implemented, where a lot of interaction with materials science is involved. The developed understanding of single phases and complex interfaces in materials is optimally used in multi-scale homogenization techniques, where it is aimed to predict the collective multi-phase response of materials. Thereby, large deformations, damage and cracking, phase transformations, etc can be taken into account.

In the past decade, substantial progress was made in the multi-scale modelling of heterogeneous materials and structures. A vast amount of literature nowadays exists, involving analytical homogenization (or coarse graining) techniques of heterogeneous elastic and inelastic materials (Ponte Castañeda 1992, Suquet 1993, Ponte Castañeda 2002, Luciano and Willis 2005), asymptotic homogenization techniques (Chung *et al* 2001, Fish and Chen 2001, Clayton and Chung 2006) and more recently variational multi-scale methods (Hughes *et al* 1998, Garikipati and Hughes 2000, Volker *et al* 2006). Among the techniques developed, one of the most powerful methods is undoubtedly computational homogenization (Suquet 1985, Ghosh *et al* 1996, Smit *et al* 1998, Miehe *et al* 1999a, Miehe *et al* 1999b, Feyel and Chaboche 2000, Terada *et al* 2000, Ghosh *et al* 2001, Kouznetsova *et al* 2001, Terada and Kikuchi 2001, Miehe and Koch 2002, Ebinger *et al* 2005, Cartraud and Messenger 2006). This method relies on the nested solution algorithm of two coupled boundary value problems, one at each scale, thereby providing an accurate multi-scale solution scheme.

This paper focuses on the upscaling of multi-layered structured thin sheets. Several applications are thereby envisaged: flexible displays, flexible solar cells, flexible electronics and even substructured shell structures like ship hulls. A recently developed second-order computational homogenization (Geers *et al* 2001, Kouznetsova *et al* 2002, Geers *et al* 2003, Kouznetsova *et al* 2004a, Kouznetsova *et al* 2004b) is exploited in order to establish an upscaling procedure for beam and shell-like structures. Enabling the homogenization of thin structured sheets towards macroscopic shells is thereby the main goal. The main assumptions and principles of this multi-scale approach are sketched, and two preliminary examples are given to illustrate its main characteristics. To keep the paper focused and compact, details that are strongly related to published aspects of second-order computational homogenization are not presented, since they can be easily reconstructed from the literature.

2. Computational homogenization

Computational homogenization is a multi-scale modelling technique to be used if the complexity of the geometry, mechanics or physics of a microstructure is too difficult to be dealt with using other (computationally less expensive) methods. The technique is essentially based on the direct extraction of the constitutive behaviour from the heterogeneity of a material, through the adequate construction and solution of a boundary value problem on a representative volume element (RVE) (Hill 1963, Drugan and Willis 1996). This technique relies on the nested solution of two boundary value problems, one for each scale. The main features and

characteristics of a computational homogenization strategy are as follows.

- No assumptions are made with respect to the constitutive response at the macro scale. The macroscopic constitutive behaviour results directly from the homogenized response of the micro-scale problem.
- The scale transitions allow for a straightforward incorporation of physical and geometrical nonlinearities. Large displacements, large strains and rotations are well addressed under the condition that the microstructural problem is solved adequately.
- There are no *a priori* restrictions with respect to the nonlinear behaviour of the different phases in the microstructure, enabling its use for evolving microstructures.
- The scale transition casts the micro-scale problem into a classical boundary value problem, for which any appropriate solution strategy can be used, e.g. finite element method, element free Galerkin, etc.
- Macroscopic constitutive tangent operators can be obtained from the microscopic overall stiffness tensor through static condensation. Consistency is preserved through this scale transition.

2.1. First-order

Computational homogenization was first proposed in its first-order version, consistent with the principle of scale separation and thereby including first-order gradients of the macroscopic displacement field only. The resulting computational homogenization scheme fits entirely in a standard continuum mechanics framework (principle of local action) and is now well established in the literature (Suquet 1985, Ghosh *et al* 1996, Smit *et al* 1998, Miehe *et al* 1999a, Miehe *et al* 1999b, Feyel and Chaboche 2000, Terada *et al* 2000, Ghosh *et al* 2001, Kouznetsova *et al* 2001, Terada and Kikuchi 2001, Miehe and Koch 2002), where details on its implementation and various applications can be found.

2.2. Second-order

The first-order computational homogenization technique does not account for the absolute dimensions of the microstructure, which constituted the main motivation for its extension towards a second-order framework (Geers *et al* 2001, Kouznetsova *et al* 2002, Geers *et al* 2003, Kouznetsova *et al* 2004a, Kouznetsova *et al* 2004b). It was realized that consistent with closed-form continuum models, a first-order approach could not account for size effects, large deformation gradients and/or macroscopic localization. More complex deformation modes, like bending, can only be incorporated if a characteristic size is involved in the scale transition.

A second-order computational homogenization scheme is obtained through the generalization of the first-order case. The coupling between the kinematics of both scales relies on a Taylor series expansion of the classical nonlinear deformation map, $\vec{x} = \phi(\vec{X})$, applied to a finite material vector $\Delta\vec{x}$ in the deformed state:

$$\Delta\vec{x} = \mathbf{F}_M \cdot \Delta\vec{X} + \frac{1}{2} \Delta\vec{X} \cdot {}^3\mathbf{G}_M \cdot \Delta\vec{X} + \mathcal{O}(\Delta\vec{X}^3). \quad (1)$$

Hence, the macroscopic (coarse scale) kinematics is determined through the deformation gradient tensor $\mathbf{F}_M = (\vec{\nabla}_{0M}\vec{x})^c$ and its Lagrangian gradient ${}^3\mathbf{G}_M = \vec{\nabla}_{0M}\mathbf{F}_M$. The macro–micro-scale transition consists of the application of relation (1) to a representative part of the microstructure, such that a classical boundary value problem is obtained at the micro scale. The micro–macro-scale transition results from the Hill–Mandel condition and the application of averaging theorems. This is schematically depicted in figure 1.

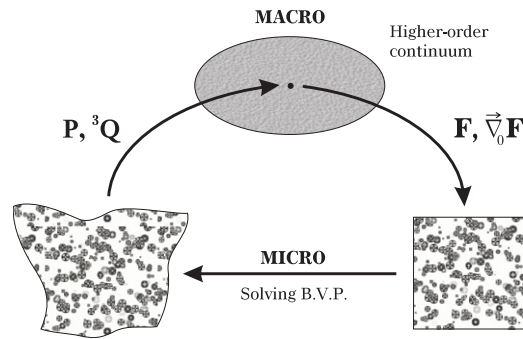


Figure 1. Second-order computational homogenization: macro-scale deformation and gradients ($F_M, {}^3G_M = \vec{\nabla}_0 F_M$) are used to solve a micro-scale boundary value problem, from which the constitutive response ($P_M, {}^3Q_M$) is extracted.

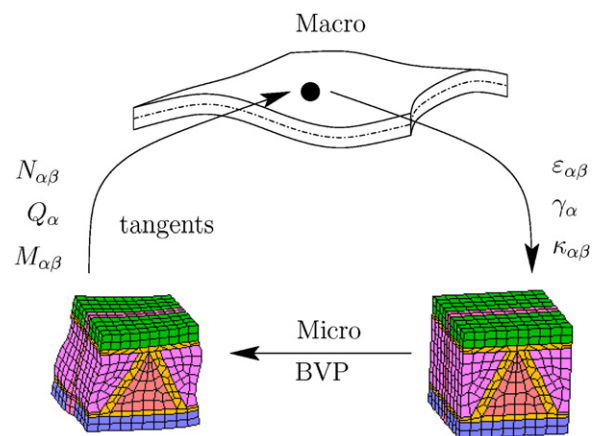


Figure 2. Shell-based computational homogenization: the macro-scale shell kinematics is used to solve a micro-scale boundary value problem on a representative volume element, from which the generalized forces of the shell are extracted.

Details of the concept of an RVE in a second-order framework are given in (Kouznetsova *et al* 2002).

3. Towards macroscopic shells

Shell problems are intrinsically of second-order type. Making use of the second-order computational homogenization scheme and applying it to shells is therefore a natural challenge. Let us consider a macroscopic shell problem, for which the constitutive response is to be extracted from its detailed substructured multi-layered composition, accounting for eventual physical and geometrical nonlinearities. The problem statement for this challenge is depicted in figure 2. For the macroscopic scale, the particular case of a Mindlin–Reisner shell will be investigated. Evidently, this choice has an influence on the scale transitions detailed below, even though the application to other shell formulations (e.g. solid-like shell) can be readily obtained in a similar manner.

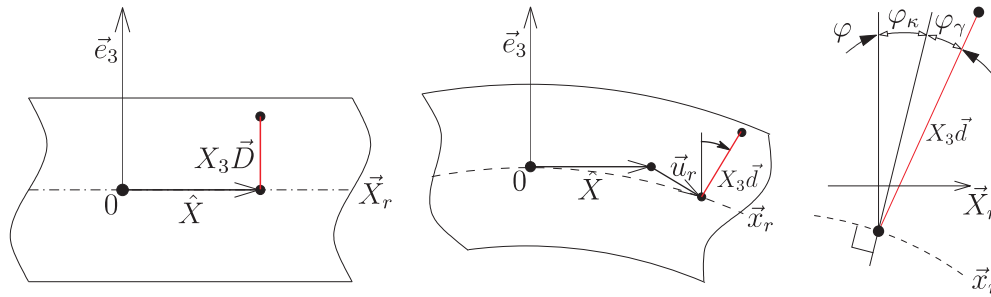


Figure 3. Mindlin–Reisner kinematics: rotations due to curvature (φ_κ) and transverse shear (φ_γ).

3.1. Macro–micro-scale transition

Let us consider a Mindlin–Reisner shell at the macro scale. The main kinematical assumptions (or rather restrictions) are highlighted in figure 3. The undeformed configuration is characterized through the position vector in the reference plane $\vec{X}_r = \hat{X}$ and the out-of-plane director \vec{D} . The position vector of an arbitrary point is then given by

$$\vec{X} = \hat{X} + X_3 \vec{D}, \tag{2}$$

in which X_3 is the out-of-plane coordinate measured along \vec{e}_3 . Upon deformation of the shell, the new current configuration is described by

$$\vec{x}^*(\vec{X}) = \vec{x}_r^*(\vec{X}_r) + X_3 \vec{d}(\vec{X}_r). \tag{3}$$

Characteristic of the Mindlin–Reisner shell, the director in the deformed configuration \vec{d} is rotated with respect to the original director through the rotation of the reference plane φ_κ (bending) and a rotation due to transverse shear φ_γ , see figure 3. The directors are assumed to remain straight and inextensible, i.e.

$$\|\vec{D}\| = \|\vec{d}\| = 1. \tag{4}$$

Furthermore, it is assumed that the stress components normal to the reference plane vanish (plane stress condition).

Next, the higher-order kinematics given by (1) is related to the Mindlin–Reisner shell kinematics. Taking the in-plane gradient of (3) and making use of the definition of \mathbf{F} permits to express the macroscopic deformation gradient tensor for the shell problem:

$$\mathbf{F}_M = \left[\underbrace{(\hat{\nabla}_{0M} \vec{x}_r)^c}_{\sim \varepsilon_{\alpha\beta}} + \underbrace{\vec{d} \vec{e}_3}_{\sim \gamma_\alpha} \right]_{\vec{X}=\vec{0}}, \tag{5}$$

in which $\hat{\nabla}_0$ represents the surface gradient operator (i.e. the in-plane part of the gradient operator, with respect to the reference plane) $\hat{\nabla} = \nabla \cdot \hat{\mathbf{I}}$, with $\hat{\mathbf{I}} = \mathbf{I} - \vec{e}_3 \vec{e}_3$. Clearly, the first term of \mathbf{F}_M in (5) is the in-plane deformation tensor, which involves the in-plane strain components $\varepsilon_{\alpha\beta}$. The second term in (5) reflects the deformation of the director, which is coupled to the transverse shear strains γ_α . With respect to the co-rotational shell coordinate system, the components of \mathbf{F}_M that can be identified are denoted in the following matrix:

$$\mathbf{F}_M \rightarrow \begin{bmatrix} \varepsilon_{11} + 1 & \varepsilon_{12} & \gamma_1 \\ \varepsilon_{21} & \varepsilon_{22} + 1 & \gamma_2 \\ 0 & 0 & \bullet \end{bmatrix}. \tag{6}$$

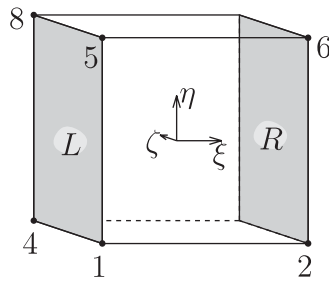


Figure 4. Through-thickness 3D RVE, with its local coordinate system.

The transverse shears are identified with the F_{13} and F_{23} components, whereas the F_{31} and F_{32} components are set equal to zero for the rotation neutralization. Note that the component F_{33} remains undetermined (due to the plane stress assumption).

Likewise, the macroscopic third-order tensor ${}^3\mathbf{G}_M$ can be obtained by taking the gradient of \mathbf{F}_M , resulting in

$${}^3\mathbf{G}_M = \vec{\nabla}_{0M}(\mathbf{F}_M) = \left[\underbrace{\vec{e}_3(\hat{\nabla}_{0M}\vec{d})^c}_{\sim\kappa_{\alpha\beta}} + \underbrace{(\hat{\nabla}_{0M}\vec{d})\vec{e}_3}_{\sim\hat{\mathbf{G}}_M} + \underbrace{\hat{\nabla}_{0M}(\hat{\nabla}_{0M}\vec{x}_r)^c}_{\sim\hat{\mathbf{G}}_M} \right]_{\vec{x}=\vec{0}}. \quad (7)$$

The first two terms of ${}^3\mathbf{G}_M$ represent the shell curvature tensor, involving the components $\kappa_{\alpha\beta}$. The third term of ${}^3\mathbf{G}_M$ is the in-plane gradient of the deformation tensor, which is not included in the shell kinematics at the macro scale, and is not transferred to the micro-scale and therefore remains undetermined. With respect to the co-rotational shell coordinate system, the corresponding components of ${}^3\mathbf{G}_M$ are denoted in the following multi-dimensional matrix:

$${}^3\mathbf{G}_M \rightarrow \left(\left[\begin{array}{ccc} \bullet & \bullet & \bullet \\ \bullet & \bullet & \bullet \\ \kappa_{11} & \kappa_{21} & \bullet \end{array} \right]^{ij1}, \left[\begin{array}{ccc} \bullet & \bullet & \bullet \\ \bullet & \bullet & \bullet \\ \kappa_{12} & \kappa_{22} & \bullet \end{array} \right]^{ij2}, \left[\begin{array}{ccc} \kappa_{11} & \kappa_{21} & \bullet \\ \kappa_{12} & \kappa_{22} & \bullet \\ \bullet & \bullet & \bullet \end{array} \right]^{ij3} \right). \quad (8)$$

The curvature components $\kappa_{\alpha\beta}$ that will be transferred from the macro shell to the micro-scale RVE are identified with the components $\kappa_{11} = G_{311} = G_{113}$, $\kappa_{21} = G_{321} = G_{123}$, $\kappa_{12} = G_{312} = G_{213}$ and $\kappa_{22} = G_{322} = G_{223}$. The in-plane strain gradients (components G_{111} , G_{121} , etc) remain undetermined, as well as the components G_{i3k} and G_{3j3} . Clearly, only a fraction of the second-order kinematics applies to the shell case presented.

Next, a representative volume element (RVE) needs to be selected. For the analysis of shells, a through-thickness RVE is taken, implying homogenization with respect to the reference plane and direct integration in the thickness direction. In the case of, e.g. a flexible display, an adequate RVE would be a single pixel, with all stacks involved. A schematic through-thickness RVE is shown in figure 4. Consistent with the developments carried out for a full second-gradient continuum in (Kouznetsova *et al* 2002), a micro-fluctuation field \vec{w} is introduced to reflect the fine-scale contribution on top of the macro-scale kinematics given by (1):

$$\Delta\vec{x} = \mathbf{F}_M \cdot \Delta\vec{X} + \frac{1}{2}\Delta\vec{X} \cdot {}^3\mathbf{G}_M \cdot \Delta\vec{X} + \vec{w}. \quad (9)$$

The first-order scale transition relation requires that the macroscopic deformation gradient $\mathbf{F}_M = (\vec{\nabla}_{0m}\vec{x})^c$ be equal to the volume average of \mathbf{F}_m . As shown in (Kouznetsova *et al* 2002),

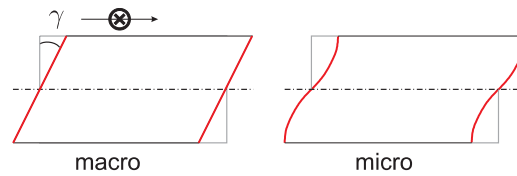


Figure 5. Macro–micro inconsistency for transverse shear γ .

this leads to the following boundary integral constraint:

$$\int_{\Gamma_0} \tilde{w} \vec{N} \, d\Gamma_0 = \mathbf{0}, \quad (10)$$

where \vec{N} is the unit outward normal on the undeformed boundary Γ_0 . Several choices can be made to enforce this boundary constraint (10). Following similar arguments as used in the elaboration of the second-order RVE, a generalized periodicity condition is used, which is based on the periodicity of the in-plane part of the micro-fluctuation field \hat{w} :

$$\hat{w}_L(s) = \hat{w}_R(s) \quad \text{and} \quad \hat{w}_F(s) = \hat{w}_B(s) \quad (11)$$

applying to the local coordinate s on opposite faces L , R (left, right) and F , B (front, back). A weak condition, satisfying (10), is introduced for the out-of-plane component of \tilde{w} :

$$\int_{\Gamma_{0L}} (\tilde{w}_R - \tilde{w}_L) \, d\Gamma_0 = \tilde{0} \quad \text{and} \quad \int_{\Gamma_{0B}} (\tilde{w}_F - \tilde{w}_B) \, d\Gamma_0 = \tilde{0}. \quad (12)$$

The boundary conditions related to transverse shears are more delicate. In order to make a proper choice for this, a well-known kinematical inconsistency of the shell must be emphasized first. The kinematical assumptions for the shell theory are confronted by those that apply naturally in the 3D RVE in figure 5. Not surprisingly, the absence of global shear tractions in the micro-scale problem (due to the plane stress condition) inhibits the directors from remaining straight (as assumed at the macro scale). The micro-scale transverse shear cannot be constrained to remain constant at the RVE faces. In order to remedy this, a weak constraint is enforced on each of the lateral faces, requiring that the average micro-scale shear of the face be equal to the macroscopic value of the transverse shear, i.e.

$$\int_{\Gamma_{0L}} X_3 \hat{w}_L \, d\Gamma_0 = 0 \quad \text{and} \quad \int_{\Gamma_{0B}} X_3 \hat{w}_B \, d\Gamma_0 = 0. \quad (13)$$

The constraints (11), (12) and (13) constitute a set of tying relations that allow to relate the position vectors of all lateral boundary points of the RVE to the macroscopic components highlighted in (6) and (8). The elaboration of these is consistent with the boundary conditions determined in the second-order computational homogenization.

3.2. Micro-scale boundary value problem

Given the boundary conditions resulting from the macro–micro-scale transition, the boundary value problem is next completed by the additional conditions applying to the top and bottom face and the constitutive relations. In this respect, a second inconsistency between the shell kinematics and the RVE problem must be handled. As emphasized in the Mindlin–Reisner shell kinematics, the directors are inextensible, indicating that the F_{33} component in (6) is taken equal to 1. This contradicts the plane stress assumption, and the inextensibility of the directors is therefore relaxed at the micro scale. As already indicated in (6), the strain in the thickness direction is left undetermined since traction-free boundaries will be used for the top

and bottom faces of the RVE. The latter conditions are typically relevant for shells that are not loaded in the out-of-plane direction, which is the case for, e.g. flexible displays or solar cells.

The RVE boundary value problem is determined by (1) the equilibrium equation taken here in terms of the first Piola–Kirchhoff stress tensor \mathbf{P}_m ; (2) the microstructural constitutive laws for each phase, layer or material and respective interfaces; and (3) the entire set of boundary conditions on all faces, as described previously.

3.3. Micro–macro-scale transition

Since the shell problem was here cast in the framework of a previously developed second-order scheme, the micro–macro-scale transition does not require special attention. All averaging relations based on the Hill–Mandel condition, as developed in (Kouznetsova *et al* 2002), apply and permit to extract a macroscopic stress tensor \mathbf{P}_M and a higher-order stress tensor ${}^3\mathbf{Q}_M$. The generalized forces (stress resultants) in the shell are obtained by direct integration of these stress components over the thickness H of the shell, leading to

$$N_{\alpha\beta} = \int_{-H/2}^{H/2} \mathbf{P}_m^{\alpha\beta} dX_3 = H \mathbf{P}_M^{\alpha\beta} \quad (14)$$

for the membrane forces $N_M^{\alpha\beta}$,

$$V_\alpha = \frac{1}{2} \int_{-H/2}^{H/2} (\mathbf{P}_m^{3\alpha} + \mathbf{P}_m^{\alpha 3}) dX_3 = \frac{1}{2} H (\mathbf{P}_M^{3\alpha} + \mathbf{P}_M^{\alpha 3}) \quad (15)$$

for the shear forces V_α and

$$M_{\alpha\beta} = \int_{-H/2}^{H/2} X_3 \mathbf{P}_m^{\alpha\beta} dX_3 = H (\mathbf{Q}_M^{3\alpha\beta} + \mathbf{Q}_M^{\beta\alpha 3})$$

for the bending/twisting moments. In all the cases, the indices α and β take values 1 and 2.

3.4. FE solution strategy

The parallelism with the full gradient continuum case also holds for the full finite element solution strategy. Equations given can be cast in a discrete form, involving finite element nodes only, see (Kouznetsova *et al* 2004b) for more details on these procedures. The macroscopic tangents, relating the generalized shell forces to the shell generalized strains, can be obtained through the static condensation of the tangent matrix of the RVE problem. These elaborations are laborious, yet well documented in the literature. Nevertheless, special care needs to be taken to properly implement the homogenized results in an existing macroscopic shell element, e.g. to properly handle local coordinate systems, rotations, etc.

4. Preliminary examples

4.1. Substructured beam

A first, straightforward case is the multi-scale analysis of the bending of a substructured beam, with length $L = 50$ mm, width $W = 2$ mm and thickness $T = 1$ mm, loaded with a point load at its extremity. This simple 2D example illustrates the direct application of the theoretical principles sketched above, in a planar analysis. The through-thickness RVE is a solid with an oblique perforation in its centre. A standard elasto-plastic von Mises model is used for the material behaviour, with a Young's modulus $E = 100$ GPa, a Poisson's ratio $\nu = 0.3$,

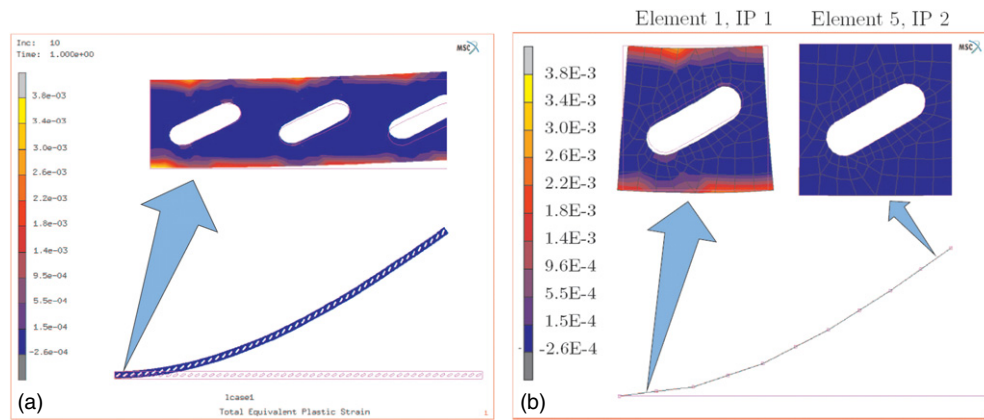


Figure 6. Multi-scale analysis of a 2D perforated beam structure: macroscopic deformation and local distribution of the total equivalent plastic strains. (a) Reference solution, (b) multi-scale solution.

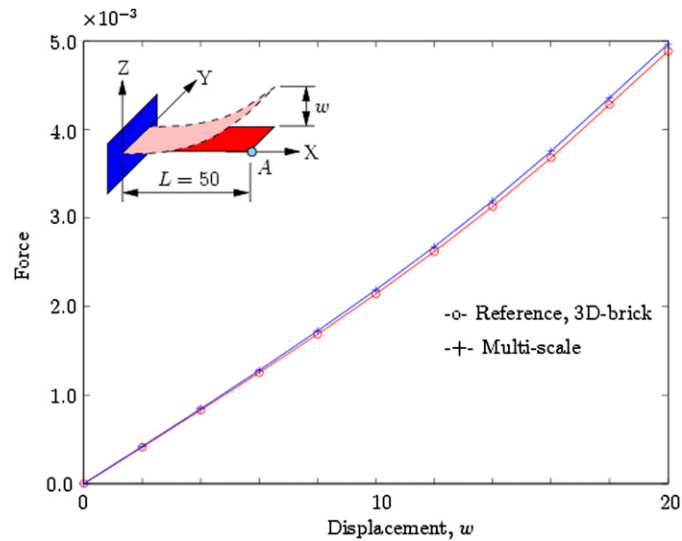


Figure 7. Multi-scale analysis of a 2D perforated beam structure: global force-displacement curve (force in (kN), displacements in (mm)).

a yield stress $\sigma_y = 1$ GPa and a linear hardening with modulus $H = 10$ GPa. The multi-scale problem is solved with 5 beam elements only, see figure 6(b). The full-scale reference solution (computed with 3D brick elements), with its equivalent plastic strain distribution is shown in figure 6(a). The comparison between the reference solution 6(a) and the multi-scale solution 6(b) is remarkable, both globally and locally at the RVE level (plastic strain distribution). The resulting applied force is shown for both approaches (full-scale reference and multi-scale) in figure 7, again emphasizing the accuracy of the multi-scale approach. Evidently, the multi-scale analysis is considerably less expensive than the full-scale analysis. Note that, consistent with (Cartraud and Messenger 2006), this methodology also allows to extract the elastic stiffness operator, if a purely elastic beam is considered.

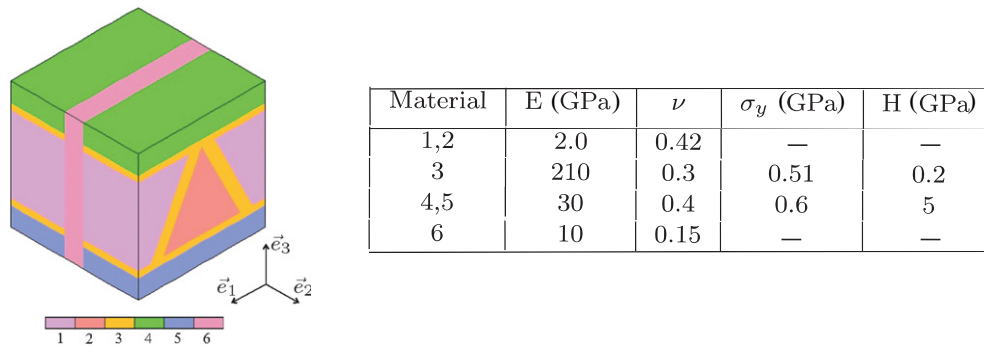


Figure 8. Through-thickness 3D RVE, substructured with 6 materials.

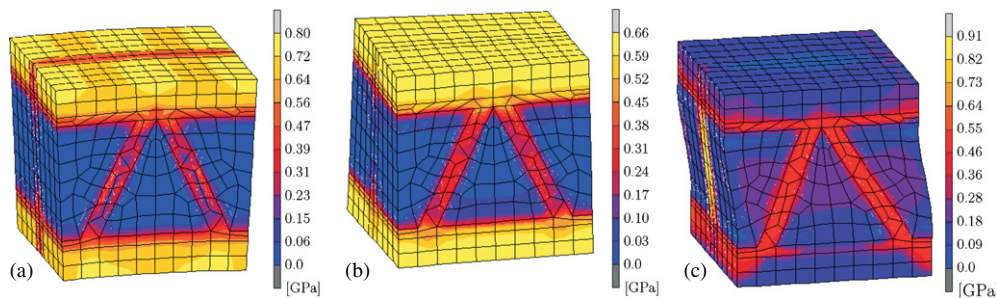


Figure 9. RVE deformations and distribution of the equivalent von Mises stress. (a) Bending $\kappa_{11} = 0.1/\text{mm}$, (b) twisting $\kappa_{12} = 0.1/\text{mm}$, (c) shearing $\gamma_{13} = 0.1$.

4.2. Substructured shell

In order to illustrate the full shell case, a periodic structure is considered composed of cubic 3D RVEs with a complex through-thickness substructure, see figure 8, composed of elasto-plastic (von Mises) materials with linear hardening H . The $1 \times 1 \times 1 \text{ mm}^3$ RVE is discretized with 8-node 3D brick elements.

Considering three typical macroscopic deformation modes, i.e. bending, twisting and shearing, the deformed RVEs and the accompanying von Mises stresses in the RVE are shown in figure 9. Note the pronounced heterogeneities throughout the different layers for the different loading cases, which cannot be captured in a closed-form homogenization of the RVE response. To further emphasize this, the most relevant associated generalized forces (per unit width) obtained through the homogenization of the RVE are visualized as well in figure 10. The nonlinear evolution of the generalized forces and their mutual presence in each of the loading cases is apparent. Each of the fine scale interactions presented is now naturally incorporated at the macro scale.

5. Conclusions

This paper addressed the main principles needed to construct a computational homogenization scheme, that links up macroscopic shells to 3D through-thickness microstructural RVEs. Particular emphasis was put on the extraction of this framework from a second-order solid–solid computational homogenization framework. It was shown that the main differences reside in the

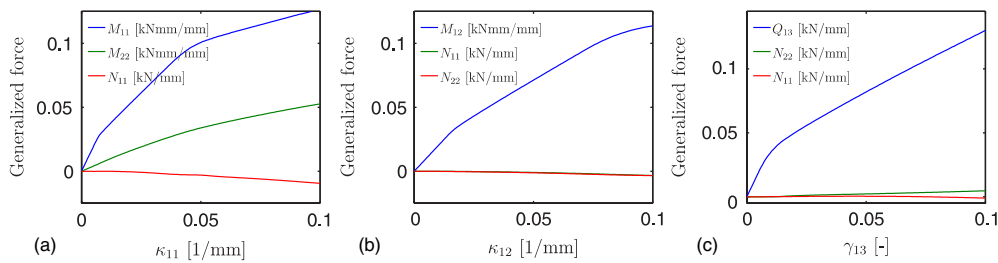


Figure 10. Macroscopic homogenized response for different RVE deformation modes. (a) Bending, (b) twisting, (c) shearing.

inherent kinematical assumptions made in the shell theory, for which adequate approximations need to be made in its 3D RVE representation. Though rather lengthy, the homogenization and the extraction of the tangent operators is structurally similar to the solid–solid framework. It therefore suffices to carry out the integration through the thickness to obtain the corresponding generalized forces and tangents for the macroscopic shell.

The resulting scheme provides a generalized force response that combines the homogenized response in the shell reference plane with a direct (RVE-based) integration through the thickness of the shell. Furthermore, the micro-scale deformation is resolved simultaneously, which is particularly relevant for multi-scale analyses and design. Consistent with existing computational homogenization frameworks, a two-scale nested numerical solution is thereby available that solves both scales concurrently. A fully coupled 2D example was shown, reflecting the bending of a substructured beam, as well as the analysis of different 3D deformation modes within the context of a 3D shell response. Further emphasis on computational details and the handling of geometrical nonlinearities within specific shell formulations will be handled in a forthcoming work.

References

- Cartraud P and Messenger T 2006 *Int. J. Sol. Struct.* **43** 686–96
- Chung P W, Tamma K K and Namburu R R 2001 *Composites A: Appl. Sci. Manuf.* **32** 1291–301
- Clayton J D and Chung P W 2006 *J. Mech. Phys. Solids* **54** 1604–39
- Drugan W J and Willis J R 1996 *J. Mech. Phys. Solids* **44** 497–524
- Ebinger T, Steeb H and Diebels S 2005 *Comput. Mater. Sci.* **32** 337–47
- Feyel F and Chaboche J L 2000 *Comput. Methods Appl. Mech. Eng.* **183** 309–30
- Fish J and Chen W 2001 *J. Eng. Mech.* **127** 1223–30
- Garikipati K and Hughes T J R 2000 *Comput. Methods Appl. Mech. Eng.* **188** 39–60
- Geers M G D, Kouznetsova V G and Brekelmans W A M 2001 *J. Physique IV* **11** 145–52
- Geers M G D, Kouznetsova V G and Brekelmans W A M 2003 *Int. J. Multiscale Comput. Eng.* **1** 371–86
- Ghosh S, Lee K and Moorthy S 1996 *Comput. Methods Appl. Mech. Eng.* **132** 63–116
- Ghosh S, Lee K and Raghavan P 2001 *Int. J. Sol. Struct.* **38** 2335–85
- Hill R 1963 *J. Mech. Phys. Solids* **11** 357–72
- Hughes T J R, Feijóo G R, Mazzei L and Quincy J 1998 *Comput. Methods Appl. Mech. Eng.* **166** 3–24
- Kouznetsova V G, Brekelmans W A M and Baaijens F P T 2001 *Comput. Mech.* **27** 37–48
- Kouznetsova V G, Geers M G D and Brekelmans W A M 2002 *Int. J. Numer. Methods Eng.* **54** 1235–60
- Kouznetsova V G, Geers M G D and Brekelmans W A M 2004a *Comput. Methods Appl. Mech. Eng.* **193** 5525–50
- Kouznetsova V G, Geers M G D and Brekelmans W A M 2004b *Int. J. Multiscale Comput. Eng.* **2** 575–98
- Luciano R and Willis J R 2005 *J. Mech. Phys. Solids* **53** 1505–22
- Miehe C and Koch A 2002 *Arch. Appl. Mech.* **72** 300–17
- Miehe C, Schotte J and Schröder J 1999a *Comput. Mater. Sci.* **16** 372–82

- Miehe C, Schröder J and Schotte J 1999b *Comput. Methods Appl. Mech. Eng.* **171** 387–418
- Ponte Castañeda P 1992 *J. Mech. Phys. Solids* **40** 1757–88
- Ponte Castañeda P 2002 *J. Mech. Phys. Solids* **50** 737–57
- Smit R J M, Brekelmans W A M and Meijer H E H 1998 *Comput. Methods Appl. Mech. Eng.* **155** 181–92
- Suquet P M 1985 Local and global aspects in the mathematical theory of plasticity, *Plasticity Today: Modeling, Methods and Applications* eds: A Sawceuk and G Bianchi (London: Elsevier Applied Science Publishers) pp 279–310
- Suquet P M 1993 *J. Mech. Phys. Solids* **41** 981–1002
- Terada K, Hori M, Kyoya T and Kikuchi N 2000 *Int. J. Sol. Struct.* **37** 2285–311
- Terada K and Kikuchi N 2001 *Comput. Methods Appl. Mech. Eng.* **190** 5427–5464
- Volker J, Songul K and William L 2006 *Comput. Methods Appl. Mech. Eng.* **195** 4594–603